Egypt. J. Chem. **Vol. 68**, No. 5 pp. 371 - 388 (2025)

Egyptian Journal of Chemistry

http://ejchem.journals.ekb.eg/

The Corrosion Inhibition Study of the Heat Exchanger Components in Chemical Cleaning Process Using the Synthesized New Cationic Gemini Surfactant

M.Mohammed[a], E.M.Ezzo[a], M.A. Hegazy[b] S.B.Mahmoud[a]*

[a]*Faculty of women for art, Science and Education, Ain Shams University, Heliopolis 11757, Cairo, Egypt*
[b]*Egyptian Petroleum Research Institute (EPRI), Nasr City, 11727 Cairo, Egypt*

Abstract
Various methods, including electrochemical impedance spectroscopy (EIS), weight loss, and potentiodynamic polarization (PP) were employed to synthesize, characterize, and asses the effectiveness of a new cationic gemini surfactant that serves as a carbon-steel (CS) corrosion inhibitor in 1 M HCl at 25-80°C. Based on the results, it was determined that the newly synthesized cationic gemini surfactant effectively inhibits CS in 1 M HCl. Raising the inhibitor's concentration and lowering the temperature may enhance the inhibition's efficiency. An investigation was conducted into the properties of activation and adsorption. The Langmuir adsorption isotherm has been discovered to be effective for inhibitor adsorption. The inhibitor is mixed-type inhibitor, according to potentiodynamic polarization tests. EDX and SEM confirmed revealed CS surface morphology.

Keywords: Cationic surfactant; Carbon steel; EIS; Tafel; and EDX; Acid inhibition.

1. Introduction

Metals and alloys undergo a transformation into more stable compounds, like sulfides, oxides, and hydroxides, when they directly interact with the environment. Corrosion is a natural process [1]. Corrosion affects several industries, most notably the oil and gas sector, and poses a hazard to public safety. Corrosion is an essential field of study [2, 3]. Carbon steel is typically regarded as the most important and extensively utilized engineered material across several sectors. Carbon steel is frequently employed because of its affordability and exceptional mechanical properties [4-8]. Mineral acids, including hydrochloric and sulfuric acids, are corrosive chemicals that can cause damage to carbon steel. Hydrochloric acid is commonly used in different applications, including equipment cleaning, rust removal, pickling, petrochemical operations, and acidifying oil wells in oil production [9-12].

Applying organic inhibitors is a remarkably efficient approach to prevent corrosion in carbon steel. However, there are numerous alternative approaches available as well. These organic inhibitors consist of surfactant molecules that have two distinct parts. One component gets pulled towards polar solvents, whereas the other component is drawn towards non-polar solvents. Head groups are frequently absorbed onto metal surfaces to construct a seamless film that provides a barrier of protection against corrosive ions in corrosive situations environments. Adsorption rate and metal surface coverage are important factors in determining the efficiency of organic inhibitors. These materials are rich in oxygen, nitrogen, and sulfur, in addition to π electrons, which enhance their adsorption affinity [13, 14].

Surfactants consist of two basic components: the water-loving "head" and the water-hating "tail." Surfactant molecules within a solution can be either physically adsorbed on a metal surface (electrostatic adsorption) or chemically adsorbed (chemisorption). The specific type of attachment is selected by the surface's charge and the free energy change that occurs when a chain of hydrocarbons moves from liquid to solid. Understanding the impact of surfactant adsorption on metal anticorrosion properties is crucial [15].

Our research investigates how well our surfactant inhibits corrosion with 1 M HCl. potentiodynamic polarization, Weight loss, and electrochemical impedance technologies will be employed to assess its inhibitive performance against CS corrosion. The influence of temperature was studied in great detail, leading to the derivation and exposition of several thermodynamic functions.

*Corresponding author e-mail: samar.belal@women.asu.edu.eg.; (Samar Belal Mahmoud).
Received date 20 August 2024; Revised date 14 September 2024; Accepted date 21 September 2024
DOI: 10.21608/ejchem.2024.313691.10229

2. Experimental

2.1. Carbon steel

The chemical constituents for the CS sample employed for this investigation appear as follows (wt.%): 0.022% Cu, 0.05% Si, 0.94% Mn, 0.004% S, 0.19% C, 0.014% Ni, 0.009% P, 0.009% Cr, 0.003% Ti, 0.034% Al, 0.016% V, and the remaining Fe.

2.2. Solutions

In this study, analytical grade 36% HCl was diluted by distilled water to generate 1 M HCl. The cationic surfactants utilized have been produced at concentrations that vary from 1 x 10^{-4} to
5 x 10^{-3} M.

2.3. Synthesis of novel cationic gemini surfactants

Fig. 1 displays the final product of the new cationic gemini surfactant that was utilized in this work. The two-step process was carried out in the following manner:

In the first step:

The Schiff base compound namely: (1E, 1'Z)-N, N'-(ethane-2-diyl) bis(1-(pyridine-4-yl) ethan-1-imine) was synthesized using a condensation reaction between 1-(pyridine-4-yl) ethan-1-one (24.228 g, 0.2 mol) and ethane-1,2-diamine (6.010 g, 1 mol) in ethanol for 4 hours at 80 °C. The product was permitted to cool. The solid had been purified using diethyl ether and subsequently recrystallized using pure ethanol.

In the second step:

The cationic gemini surfactant namely: 4,4'-((1Z,1'E)-(ethane-1,2-diylbis(azaneylylidene)bis(ethane-1-yl-1-ylidene))bis(1-dodecylpyridin-1-ium) bromide was synthesized through quaternization reaction of the product of first step (Schiff base (I)) (5.327 g, 0.2 mol) and 1-bromododecane (9.9696 g, 0.4 mol) in ethanol for 72 hours at 80°C. The product was permitted to cool. The solid had been purified using diethyl ether and subsequently underwent recrystallization using pure ethanol.

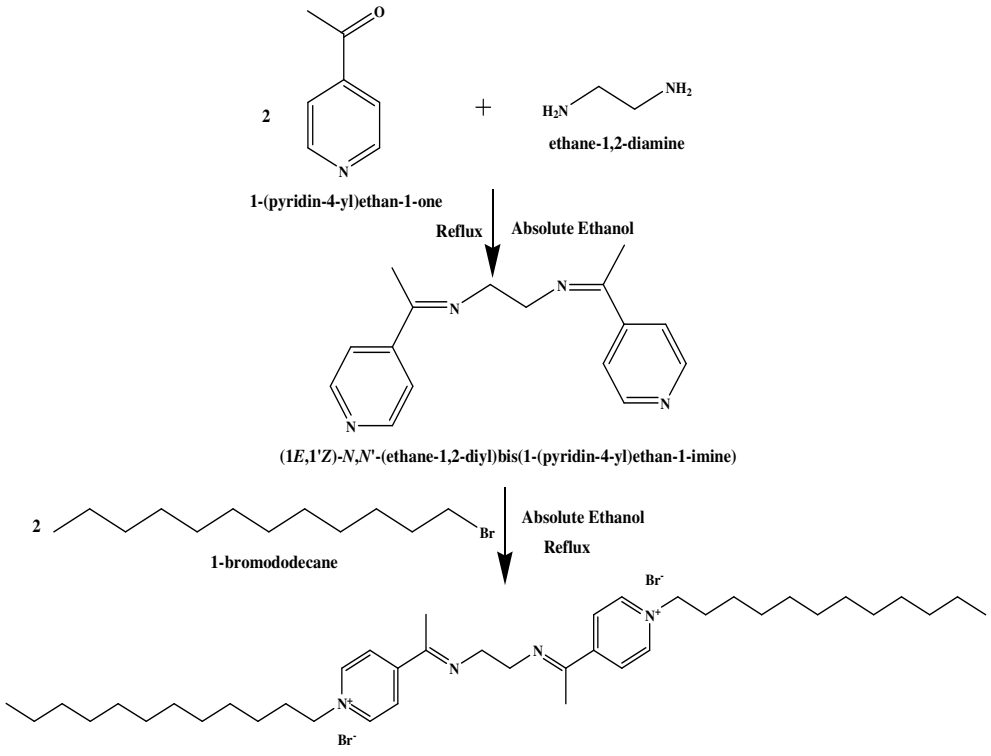

Figure 1: Preparation of the novel cationic gemini surfactant.

2.4. Surface tension measurements

Using a Du Nouy Tensiometer (Kruss Type 6), the surface tension of the produced CGS was measured at various concentrations. We created all solutions with high-quality double-distilled water and all-glass equipment. At 25 °C, the water had a surface tension equals 72 mN cm^{-1}.

2.5. Weight loss technique

Using various grades of emery paper (320-400-800-1000-1200), the CS specimens, measuring 6 cm × 3 cm × 0.4 cm, were carefully abraded. Afterward, they were thoroughly cleaned with distilled water and acetone. 100 ml of 1.0 M HCl was added to a closed beaker containing the samples. Various amounts of the manufactured inhibitor were added to some of the samples. The temperatures ranged from 25–80 °C. The samples were accurately weighed before being immersed. Temperature was regulated to ±1°C using a water bath and thermostat. After 24 hours, the C-steel specimens were eliminated. After removing any grease by using acetone, the specimens were rinsed twice utilizing distilled water. They were then submerged for 10 seconds in a fluid of 1.0 M HCl to remove any rust compounds. After drying thoroughly, they were weighed accurately, and an average value was obtained by repeating the experiment three times. Subsequently, the experiments were replicated at different temperatures.

2.6. Electrochemical method

Electrochemical investigations were performed with a cell containing three electrodes, employing a saturated calomel electrode (SCE) and a platinum counter electrode (CE) as reference electrodes. For the experiment, A CS rod was placed into a PVC holder with precision, secured firmly with epoxy glue. The flat surface of the rod was used as the contact area for the electrode prior to every measurement, at an open circuit potential (OCP), to attain the steady state, The electrode had been submerged in the testing liquid for approximately 30 minutes. The time was set considering many parameters, including when the C-steel electrode is introduced into the test fluid. The OCP undergoes immediate change but eventually stabilizes. The potential being referred to is commonly referred to as the equilibrium or corrosion potential. Using a Voltalab 40 PGZ 301 potentiometer and a computer with Voltamaster 4 software. All polarization curves were successfully recorded at 25 °C.

For potentiodynamic polarization measurement, the potential of the electrodes altered immediately from -800 mV to -300 mV against SCE at the OCP. This was carried out at 25°C with a scan rate of 0.2 mV s^{-1}. The electrochemical impedance spectroscopic measurement was performed following the previously provided description. At a temperature of 25 °C, the cell experienced a minor voltage fluctuation (10 mV) that alternated at frequencies varying from 100 kHz to 30 mHz [16, 17].

2.7. Surface analysis

2.7.1. EDX

The surface morphology of polished C-steel was studied using energy dispersive X-rays (EDX). Looking at the elemental composition of C-steel surfaces that have been polished or corroded in the presence or absence of inhibitors using both inhibited and uninhibited samples. Before being polished, rinsed with distilled water, after being soaked in acidic solutions, inhibitors or not, the steel was left to dry at the ambient temperature. [30].

2.7.2. Scanning electron microscopy (SEM):

Using SEM (Jeol, 5400, Japan) which considers a powerful tool used for surface examination in absence and presence of high concentration of $5x10^{-3}$ M of Schiff base, and cationic gemini surfactant (CGS)), C-steel was dissolved in a 1 M HCl solution for 24 hours. The images of the inhibited and uninhibited sample were carried out at a magnification of X = 1000 and using energy acceleration beam 30 kV.

3. Results and Discussion

3.1. Characterization of the produced compounds

3.1.1. Characterization of the produced Schiff base compound

The structure of the produced Schiff base (1) was confirmed using FTIR, ^{1}HNMR, and mass spectroscopy.

3.3.1.1. FTIR Spectroscopy

The produced Schiff base (I) compound's FTIR spectra **(Fig. 2)** displayed a spectrum of absorption: at 3059 cm^{-1} (C-H aromatic), 2915.46 cm^{-1} (C-H asymmetric stretching), 2892.00 cm^{-1} (C-H symmetric stretching), 1664.90, 1627.47 cm^{-1} (C=N stretching), 1597.22, 1546.09 cm^{-1} (C=C stretching), 827.38 (C-H alkene bend), 754.46 cm^{-1} (CH_2 rocking), 1369.15 cm^{-1} (CH_3 bending), 1412.63 cm^{-1} (CH_2 bending).

3.3.1.2. ^{1}HNMR Spectroscopy

The produced Schiff base (I) compound's ^{1}HNMR (DMSO-d6) spectra **(Fig. 3)** displayed many peaks at δ (ppm): 2.265 (s, 6H, $CH_2N=C\underline{\mathbf{H}}_3$), 3.888 (d, 4H, $C\underline{\mathbf{H}}_2N=CH3$), 7.703-7.718 (d, 4H, m-pyridine), 8.604-8.623 (d, 4H, o-pyridine).

3.3.1.3. Mass Spectroscopy

The produced compound's mass spectra **(Fig. 4)** showed a base beak and molecular ion peak at m/z (%); 265.06 (100%, $C_{16}H_{18}N_4$). Fragmentation as follows: 188.11 (1.86%, $C_{11}H_{14}N_3^+$), 53.03 (4.12%, $C_3H_3N^+$).

3.3.2. Structure characterization of the synthesized cationic gemini surfactant compound

3.3.2.1. FTIR Spectroscopy

The cationic gemini surfactant's FTIR spectra **(Fig. 5)** revealed the subsequent absorption bands.

: at 2923.43 cm^{-1}(C-H asymmetric stretching) and 2852.67 cm^{-1} (C-H symmetric stretching) for 3119.09 and 3040.74 cm^{-1} (C-H aromatic), 1636.05 cm^{-1} (C=N stretching), 1562.60 cm^{-1} (C=C stretching), 1373.94 cm^{-1} (CH_3 bending), 1465.54 cm^{-1} (CH_2 bending), 721.25 cm^{-1} (CH_2 rocking), 1049.58 cm^{-1} (C-N^+).

3.3.2.2. ^{1}HNMR Spectroscopy

The produced cationic gemini surfactant's ^{1}HNMR (DMSO-d6) spectra **(Fig. 6)** showed several peaks at δ (ppm): 0.843 (t, 6H, $NCH_2(CH_2)_{10}C\underline{\mathbf{H}}_3$), 1.227 (m, 40H, $NCH_2(C\mathbf{H}_2)_{10}CH_3$), 1.904 (s, 6H, N=C-C$\underline{\mathbf{H}}_3$), 4.50 (t, 4H, $NC\underline{\mathbf{H}}_2(CH_2)_9CH_3$), 4.59 (t, 4H, $NC\underline{\mathbf{H}}_2C\underline{\mathbf{H}}_2N$), 8.20-9.31 (d, 8H, H-pyridine).

3.3.2.3. Mass Spectroscopy

The cationic gemini surfactant's mass spectra **(Fig. 7)** displayed a molecular ion peak at m/z (%); 764.53 (1.33%) together with a base peak at 91.11 (100% $C_6H_5N^+$). Fragmentation appears as below: 43.10 (95.20%, $C_3H_7^+$), 252.12 (32.93%, $C_{15}H_{16}N_4^+$), 137.09 (22.85%, $C_8H_{13}N_2^+$), 97.16 (31.29%, $C_5H_9N_2^+$).

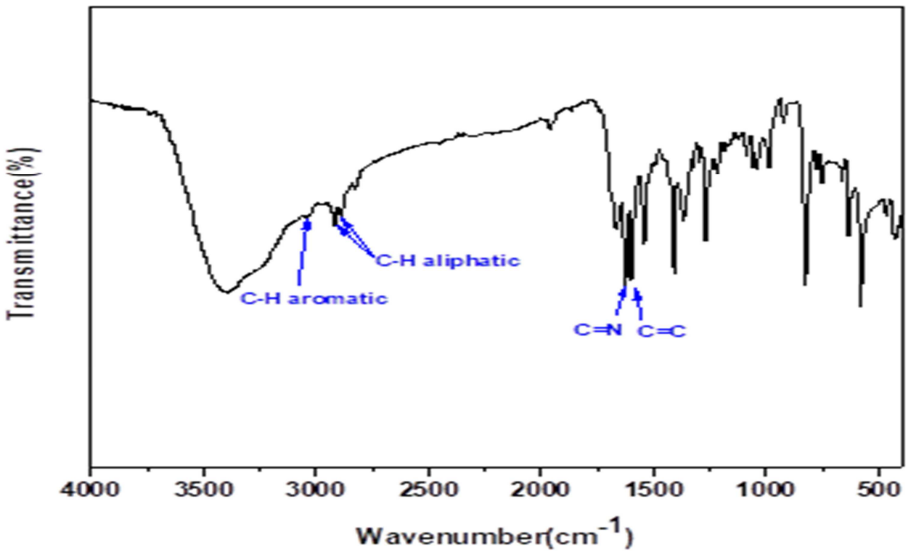

Figure 2: FTIR spectrum of the synthesized Schiff base compound.

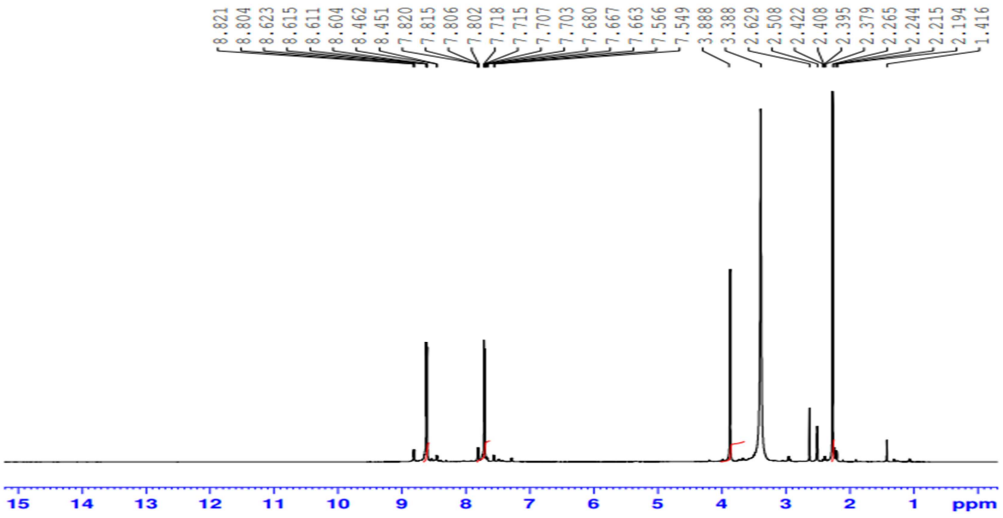

Figure 3: ^{1}HNMR spectrum of the synthesized Schiff base compound.

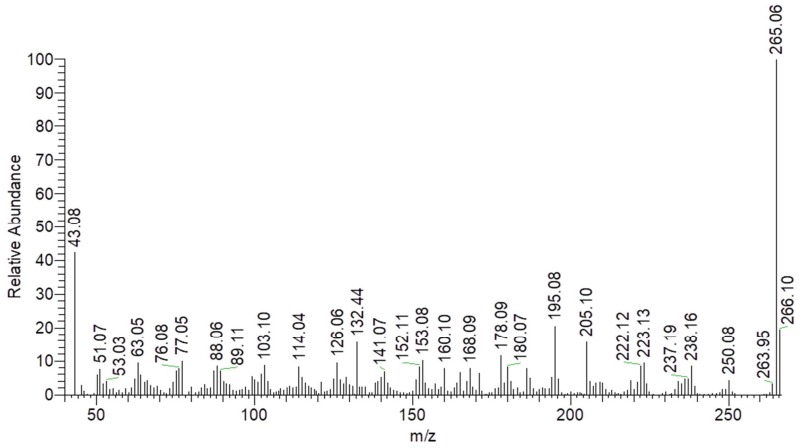

Figure 4: Mass spectrum of the synthesized Schiff base compound.

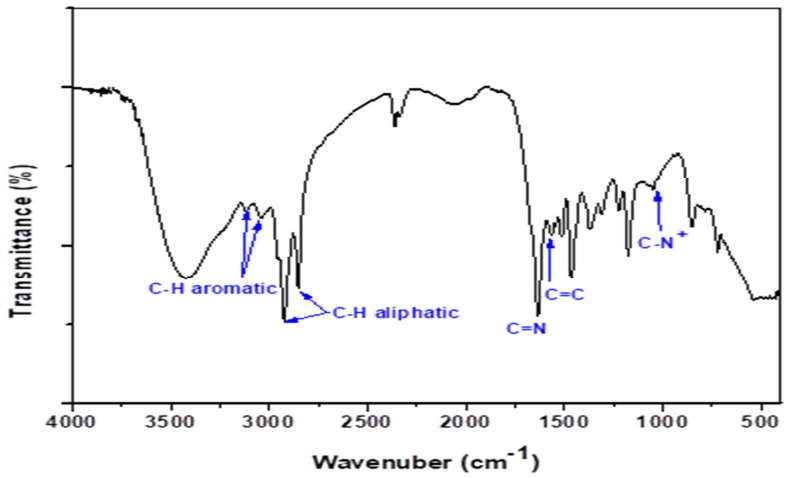

Figure 5: FTIR spectrum of the synthesized cationic gemini surfactant compound.

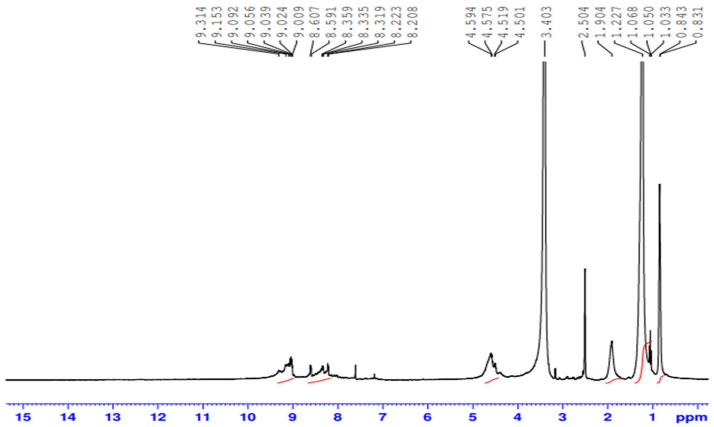

Figure 6: [1]HNMR spectrum of the synthesized cationic gemini surfactant compound.

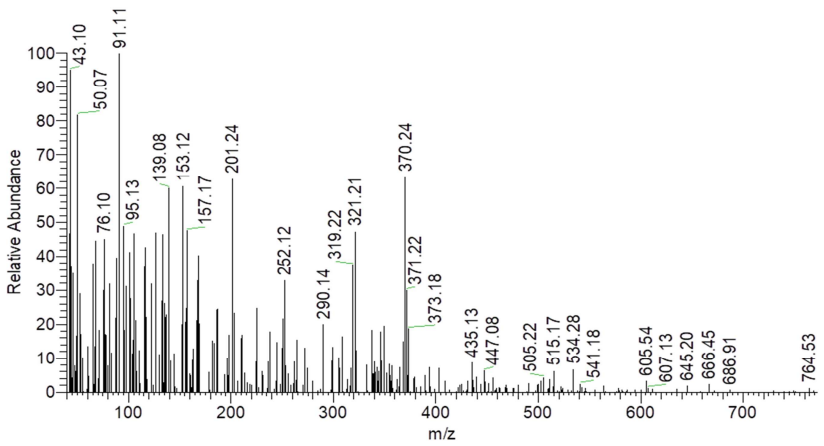

Figure 7: Mass spectrum of the synthesized cationic gemini surfactant compound.

3.2. Weight-loss measurements

3.2.1. The concentration effect

Corrosion rate (k) and inhibition efficiency (η_w) were estimated using the equations below.

$$k = \frac{\Delta W}{St} \qquad (1)$$

where ΔW = average weight loss, t = immersion period in hours, and S = specimen total area in cm^2

$$\eta_w = \frac{W_0 - W}{W_0} x\ 100 \qquad (2)$$

The equation includes the specimen's total area (S) in cm^2, the immersion period (t) in hours, and the average weight loss (ΔW).

Table 1 provides the outcomes of the weight loss procedure for various inhibitor concentrations (1.0×10^{-4} M to 5.0×10^{-3} M) and temperatures (25 °C to 70 °C), as well as the values of the corrosion rate (k). Raising the inhibitor's concentration enhances inhibition efficiency, according to our findings. Raising the inhibitor concentration results in a corresponding rise in the area occupied by adsorbed molecules, which in turn increases the efficacy of inhibition by separating the surface from the hostile medium. The inhibitor's concentration affects the corrosion rate and the efficiency of inhibition [18, 19].

3.2.2. The temperature effect

Various experimental techniques were employed to analyze how solution temperatures affect CS corrosion in the absence and presence of a synthetic surfactant. The experimental data collected is presented in Table 1. The findings indicate that the corrosion rate is significantly impacted by the temperature of the solution, irrespective of the amounts of inhibitors. As temperature increased, the activation energy of the reactive species also increased, resulting in improved electrochemical processes [8]. Although the inhibitory efficiency declined with higher temperatures, it is plausible that certain surfactant molecules were detaching from the metal surface [20].

Table 1: Weight loss results for carbon steel in 1 M HCl in the absence and presence of different concentrations of the synthesized cationic gemini surfactants at various temperatures.

Inhibitor name	Inhibitor conc. (M)	25 °C			40 °C			55 °C			70 °C		
		k (mg cm^{-2} h^{-1})	θ	η_w (%)	K (mg cm^{-2} h^{-1})	θ	η_w (%)	k (mg cm^{-2} h^{-1})	θ	η_w (%)	k (mg cm^{-2} h^{-1})	θ	η_w (%)
Absence	**1M HCl**	**0.4303**	**-**	**-**	**0.9904**	**-**	**-**	**2.0077**	**-**	**-**	**3.9413**	**-**	**-**
Schiff base	**1.0×10^{-4}**	**0.1446**	**0.66**	**66.40**	**0.3957**	**0.60**	**60.04**	**0.8585**	**0.57**	**57.24**	**1.8714**	**0.53**	**52.52**
	5.0×10^{-4}	**0.1111**	**0.74**	**74.18**	**0.3245**	**0.67**	**67.24**	**0.7423**	**0.63**	**63.03**	**1.5825**	**0.60**	**59.85**
	1.0×10^{-3}	**0.0850**	**0.80**	**80.25**	**0.2365**	**0.76**	**76.12**	**0.5567**	**0.72**	**72.27**	**1.3128**	**0.67**	**66.69**
	5.0×10^{-3}	**0.0607**	**0.86**	**85.90**	**0.1841**	**0.81**	**81.41**	**0.4497**	**0.78**	**77.60**	**1.0696**	**0.73**	**72.86**
Surfactant	**1.0×10^{-4}**	**0.1382**	**0.68**	**67.88**	**0.3528**	**0.64**	**64.37**	**0.7721**	**0.62**	**61.54**	**1.6540**	**0.58**	**58.03**
	5.0×10^{-4}	**0.1027**	**0.76**	**76.13**	**0.2745**	**0.72**	**72.28**	**0.6460**	**0.68**	**67.82**	**1.4185**	**0.64**	**64.01**
	1.0×10^{-3}	**0.0724**	**0.83**	**83.17**	**0.2131**	**0.78**	**78.49**	**0.5019**	**0.75**	**75.00**	**1.0836**	**0.73**	**72.51**
	5.0×10^{-3}	**0.0459**	**0.89**	**89.33**	**0.1427**	**0.86**	**85.60**	**0.3507**	**0.83**	**82.53**	**0.7991**	**0.80**	**79.72**

3.3. Electrochemical Measurement

3.3.1. The potentiodynamic Polarization measurements

Research analyzed cathodic and anodic kinetics with and without various concentrations of a surfactant. Tafel polarization was used to investigate C-steel behavior in a 1M HCl solution, as shown in (Fig. 8,9). Surfactant concentrations have a significant impact on cathodic and anodic curves, indicating that the surfactant has a complex influence on the inhibitors. It reduces the generation of hydrogen gas and the corrosion of metal. Table 2 contains electrochemical measurements involving inhibition efficiency (η_p), corrosion potential (E_{corr}), the current density of corrosion (i_{corr}), and slopes of Tafel (β_a, β_c). Polarization data was used to calculate inhibitory efficiency η_p (%) using equation (3):

$$\eta_p = \frac{i_{corr} - i_{corr}\ (inh)}{i_{corr}}\ x\ 100 \qquad (3)$$

where i_{corr} and i_{corr}(inh) represent the CS electrode corrosion current densities in uncontrolled and inhibited solutions, respectively. Table 2 Indicates a subtle modification in anodic and cathodic Tafel constants, β_a and β_c, indicating that the surfactant exhibits characteristics of both types, as it decelerates the cathodic hydrogen evolution process and impedes the anodic dissolution of CS. Surfactant has minimal impact on the corrosion potential (E_{corr}). This proves that adding an inhibitor does not alter the deterioration of CS in a solution that contains 1.0 M HCl. This inhibitor initially attaches to the binding sites on the CS surface, hindering their activity and decreasing the amount of surface area accessible for corrosion reactions [21, 22]. As the surfactant concentration rises, i_{corr} values decrease, showing that the surfactant in a solution containing 1.0 M HCl decreases the solubility of CS to variable degrees depending on the concentration.

Table 2: Potentiodynamic polarization parameters for CS in 1M HCl with and without different concentrations of inhibitor at 25 ^{O}C

The inhibitors	Conc. of inhibitor (M)	E_{corr} (mV vs SCE)	i_{corr} (mA cm^{-2})	β_a (mV dec^{-1})	β_c (mV dec^{-1})	η_p (%)
Blank	**0.00**	**-496.7**	**0.4512**	**169.7**	**-158.1**	**-**
Schiff base	**1x10^{-4}**	**-498.7**	**0.1551**	**167.0**	**-170.5**	**65.63**
	5x10^{-4}	**-499.3**	**0.1107**	**162.9**	**-152.9**	**75.47**
	1x10^{-3}	**-513.3**	**0.0900**	**166.5**	**-169.2**	**80.05**
	5x10^{-3}	**-510.8**	**0.0568**	**170.5**	**-169.8**	**87.41**
Surfactant	**1x10^{-4}**	**-503.9**	**0.0985**	**180.6**	**-187.5**	**78.17**
	5x10^{-4}	**-492.5**	**0.0491**	**184.3**	**-182.6**	**89.12**
	1x10^{-3}	**-508.5**	**0.0274**	**169.9**	**-139.2**	**93.93**
	5x10^{-3}	**-522.7**	**0.0198**	**182.5**	**-164.2**	**95.61**

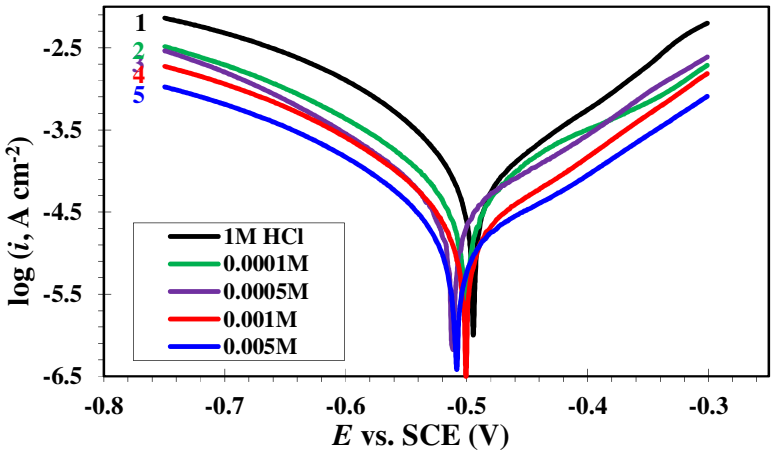

Figure 8: Potentiodynamic polarization curves for the carbon steel in 1 M HCl solution in the absence and presence of different concentrations of the Schiff base at 25 °C.

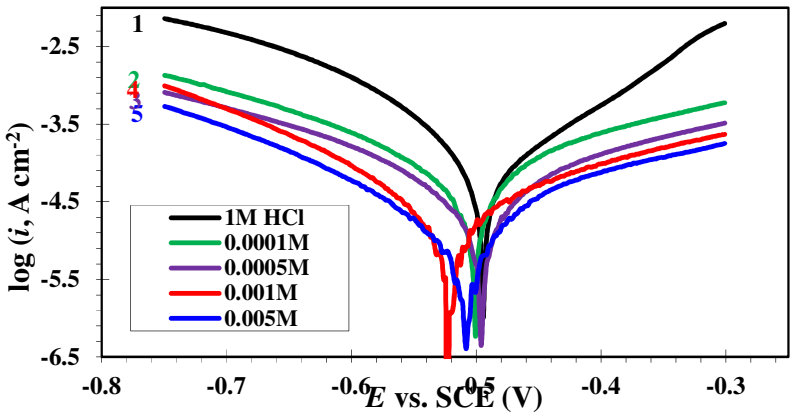

Figure 9: Potentiodynamic polarization curves for the carbon steel in 1 M HCl solution in the absence and presence of different concentrations of the cationic gemini surfactant at 25 °C.

3.3.2. Electrochemical Impedance Spectroscopic techniques (EIS)

Figs. (10a, b, 11a, b) Demonstrate the Nyquist and Bode diagrams illustrating the behavior of metal samples when subjected to a 1.0 M of HCl with inhibitors created with varying concentrations. The Nyquist plot remained the same for each tested inhibitor concentration. The findings show that inhibitor injection did not have any impact on the corrosion process. Based on the EIS theory, the high-frequency loops did not contain any full semicircles. The fluctuation seen can be attributed to the double layers that work as a capacitor don't behave perfectly. This effect is linked to the unevenness of the metallic surfaces and the correlation between frequency distribution and roughness [23]. The carbon steel/solution contact's electrochemical equivalent circuit was illustrated in Fig. 12. In order to verify the nonideal behavior, the double layer capacitance (C_{dl}) was substituted for the charge transfer resistance (R_{ct}), solution resistance (R_s), and constant phase element (CPE) in this circuit [24]. Fig. 12 displays the Nyquist and Bode simulation graphs, which may be referenced in (Figs. 10a, 10b, 11a, and 11b). Additionally, the recommended inhibitor model is also included. The ZSimpWin software was utilized to assess several parameters for the experimental data, like the proportional factor (Y_o), phase shift (n), R_s, and R_{ct}. Table 3 presented the computed EIS factors. The predicted impedance in the CPE, ZCPE case was established as shows [25-27]:

$$z_{cpE} == \frac{1}{Y_o(j\omega)^n} \qquad (4)$$

where n represents the phase shift, $J^2 = -1$, and $\omega = 2\pi f$. As previously mentioned, the double layer capacitance (C_{dl}) and a CPE were computed [28, 29] ,

$$C_{dI} = Y_o(\omega_{max})^{n-1} \qquad (5)$$

$\omega_{max} = 2\pi f_{max}$, where f_{max} = the frequency at the maximum impedance-imaginary component. The efficiency of preventing corrosion of metals was achieved, as displayed [30, 31]:

$$\eta I = \frac{R_{ct} - R_{ct}^0}{R_{ct}} x100 \qquad (6)$$

R_{ct} and R_{ct}^0: the charge transfer resistance values in the various liquids that were inhibited and those that were not inhibited simultaneously.

Fig. (10b,11b) Displays the Bode and angle phase diagram of the metallic surface in a 1M HCl solution before and after treatment with an inhibitor at different doses. The phase angle, and the logarithm of Z and f were found to be linearly related, with a slope of around -1. This relationship is evident in the Bode charts throughout the middle frequency range, where the phase angle is around -60°.The results indicated that the capacitive exhibited suboptimal performance at middle frequencies. Furthermore, while observing the data displayed by a Bode impedance slope at intermediate frequencies, if the slope is -1 with a phase angle of -90°, it indicates a perfect capacitive behavior [32]. The measurements of slope and phase angle in the solution affected by SCGS were found to be higher than those in the solution without SCGS control. This finding illustrates the inhibitory impact of the SCGS on the process of CS dissolving. Table 3 presents the results of electrochemical impedance obtained the efficacy of preventing metal corrosion (ηI) and the results of the Nyquist plots. Based on the findings in Table 3, the inclusion of SCGS at different concentrations led to an elevation in R_{ct} values and a reduction in CPE values. The CPE values decreased due to SCGS adsorption on the metallic surface. Adsorption causes an augmentation in the electric double layers and a reduction in the local dielectric constant [33].

Table 3: EIS parameters for CS in 1M HCl with and without different concentrations of inhibitor at 25 ^{O}C

The inhibitor	Conc. of inhibitor (M)	R_s (Ω cm^2)	Q_{dl} (mΩ^{-1}s^n cm^{-2})	n	R_{ct} (Ω cm^2)	$Chsq$ x10^3	C_{dl} (μF cm^{-2})	η_I (%)
Absence	**0.00**	**1.65**	**0.4448**	**0.83**	**60.75**	**0.877**	**209.5**	**-**
Schiff Base	**1x10^{-4}**	**2.12**	**0.1563**	**0.84**	**271.5**	**4.83**	**20.51**	**66.31**
	5x10^{-4}	**2.27**	**0.1251**	**0.85**	**231.9**	**5.15**	**15.95**	**73.80**
	1x10^{-3}	**3.35**	**0.0813**	**0.86**	**301.5**	**1.20**	**12.22**	**79.85**
	5x10^{-3}	**2.11**	**0.0613**	**0.85**	**418.9**	**3.81**	**8.83**	**85.50**
Surfactant	**1x10^{-4}**	**2.00**	**0.1067**	**0.80**	**280.4**	**5.81**	**13.21**	**78.33**
	5x10^{-4}	**2.22**	**0.0545**	**0.88**	**495.4**	**1.52**	**7.52**	**87.74**
	1x10^{-3}	**3.45**	**0.0345**	**0.82**	**827.7**	**1.11**	**4.51**	**92.66**
	5x10^{-3}	**2.13**	**0.0243**	**0.88**	**1122.0**	**2.53**	**3.41**	**94.59**

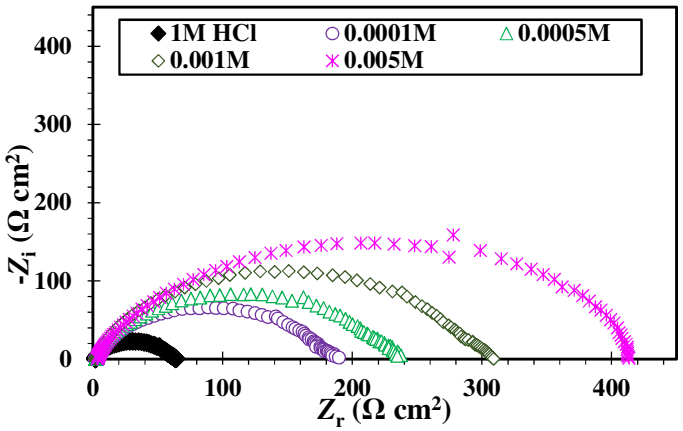

Figure 10a: Nyquist curves for the carbon steel in 1 M HCl solution in the absence and presence of different concentrations of the Schiff base at 25 °C.

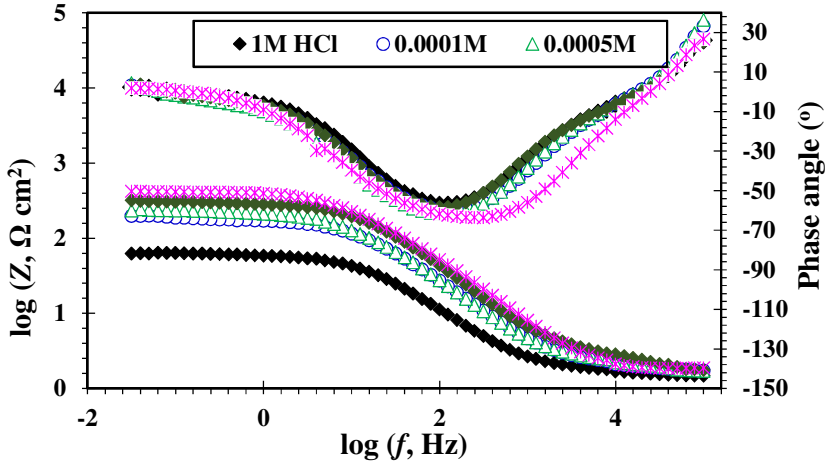

Figure 10b: Bode & Phase curves for the carbon steel in 1 M HCl solution in the absence and presence of different concentrations of the Schiff base at 25 °C.

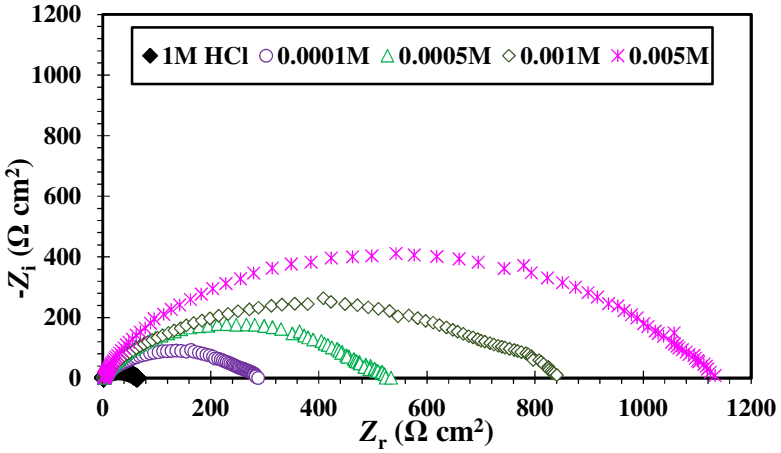

Figure 11a: Nyquist curves for the carbon steel in 1 M HCl solution in the absence and presence of different concentrations of the cationic gemini surfactant at 25 °C.

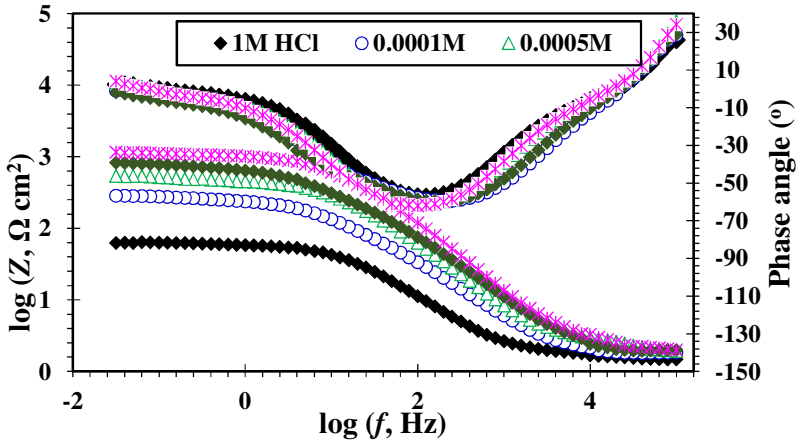

Figure 11b: Bode & Phase curves for the carbon steel in 1 M HCl solution in the absence and presence of different concentrations of the cationic gemini surfactant at 25 °C.

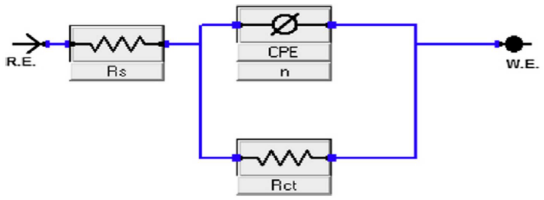

Figure 12: Electrical equivalent circuit curves for the carbon steel in 1 M HCl solution in the absence and presence of different concentrations of the tested compounds.

3.4. Adsorption isotherm and thermodynamic parameters

Adsorption isotherms supply data related to how inhibitors interact with metallic surfaces. Surface coverage (θ) value was derived utilizing the data of weight loss at 25, 40, 55, and 70°C using Equation (7):

$$\theta = \left(\frac{W_0 - W}{W_0}\right) \qquad (7)$$

W_o and W represent weight loss both without and with the inhibitor. As represented in (Fig. 13, 14), the graph of C/θ displayed against C. The data had a strong relationship that is linear, as indicated by a correlation value of 0.9999. Additionally, the slope of the line was around 1. The data suggests that the surfactant generated is adsorbed onto the CS surfaces in a solution of hydrochloric acid, Following the process of Langmuir adsorption isotherm as described with equation (8) [34-36].

$$\frac{C}{\theta} = \frac{1}{K_{\text{ads}}} + C \qquad (8)$$

In this equation. K_{ads} denotes the equilibrium constant for adsorption-desorption, C denotes the inhibitor's concentration, and θ represents surface coverage. Table 4 shows carbon steel K_{ads} values for different concentrations and temperatures. These values are determined by calculating the inverse of the intercept of isothermal lines. When temperatures are reduced, the inhibitor exhibits a strong adsorption on carbon steel. Conversely, because inhibitor desorption increases with increasing temperature, the equilibrium levels steadily fall. Equation (9) provides the relationship between adsorption constants (K_{ads}) and standard free energy ($\Delta G°_{ads}$) [25]:

$$\Delta G^0_{\text{ads}} = -RT\ln(55.5K_{ads}) \qquad (9)$$

The $\Delta G°_{ads}$ symbolizes the standard free energy, R stands for gas constant, the molar concentration of water is 55.5, and K_{ads} represents the equilibrium constant of the adsorption-desorption processes. The $\Delta G°_{ads}$ readings for the synthesized compound exhibit negativity, as indicated in Table 4. It appears that adsorption processes occur naturally and that the film formed on C-steel surfaces remains intact. When $\Delta G°_{ads}$ readings are -20 kJ mol^{-1} or higher, it suggests that charged. molecules are interacting with metal surfaces through electrostatic forces, much like a physical chemist would observe. This phenomenon is known as physisorption. When the values are −40 kJ mol^{-1} or lower, it means that the molecules of the inhibitor are transferring or sharing charges with the metal surfaces. This leads to the creation of a coordinate covalent bond, which is referred to chemisorption. Table 4 presents the $\Delta G°_{ads}$ readings, which changed from -33.49 to -40.78 kJ mol^{-1}. Adsorption of inhibitors on C-steel surfaces includes A combination of Chemical and physical reactions, Unlike the traditional techniques of adsorption, which involve both physical and chemical processes, Apply the Van't Hoff equation to compute adsorption heat ($\Delta H°_{ads}$).

$$\ln K_{ads} = \left(\frac{-\Delta H^0_{\text{ads}}}{RT}\right) + \text{const} \qquad (10)$$

The $\Delta H°_{ads}$ value is calculated by analyzing the association between ln K_{ads} and 1/T, which can be expressed as $-\Delta H°_{ads}/R$, as shown in Fig. 15. A negative value of $\Delta H°_{ads}$ implies an exothermic inhibitor adsorption operation. To determine the entropy of adsorption inhibitor ($\Delta S°_{ads}$), use this equation:

$$\Delta G^0_{\text{ads}} = \Delta H^0_{\text{ads}} - T\Delta S^0_{\text{ads}} \qquad (11)$$

Table 5 Shows the obtained $\Delta S°_{ads}$ values. When $\Delta S°_{ads}$ is positive, it indicates an increase in disorder caused by adsorbing a molecule that acts as an inhibitor and removing numerous water molecules by desorption [37, 38] .

Table 4: Standard thermodynamic parameters of adsorption on carbon steel surface in 1 M HCl containing different concentrations of the synthesized cationic gemini surfactant.

Inhibitor	Temperature (°C)	K_{ads} (M^{-1})	$\Delta G°_{ads}$ (kJ mol^{-1})	$\Delta H°_{ads}$ (kJ mol^{-1})	$\Delta S°_{ads}$ (J mol^{-1} K^{-1})
Schiff base	**25**	**13369**	**-33.49**	**-8.50**	**83.84**
	40	**10657**	**-34.59**		**83.32**
	55	**9512**	**-35.93**		**83.62**
	70	**8442**	**-37.24**		**83.76**
Surfactant	**25**	**12900**	**-33.40**	**-7.88**	**85.63**
	40	**11104**	**-34.69**		**85.65**
	55	**9507**	**-35.93**		**85.51**
	70	**8550**	**-37.27**		**85.68**

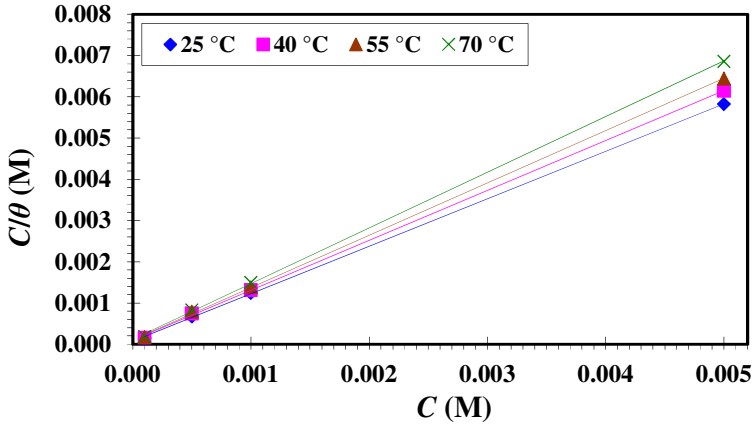

Figure 13: Langmuir adsorption plots for Schiff (1) on the carbon steel surface at various temperatures.

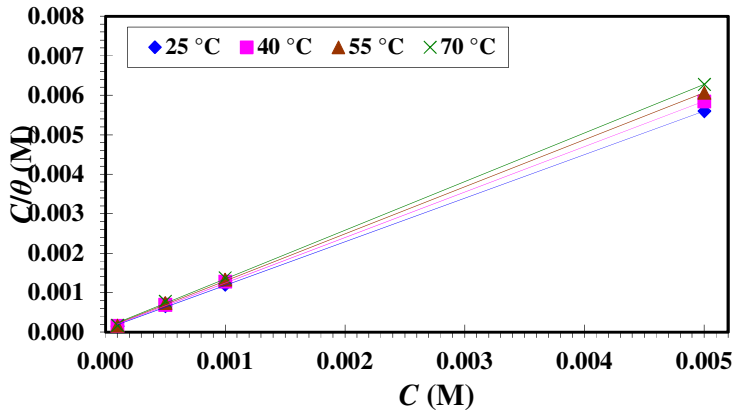

Figure 14: Langmuir adsorption plots for cationic gemini surfactant on the carbon steel surface at various temperatures.

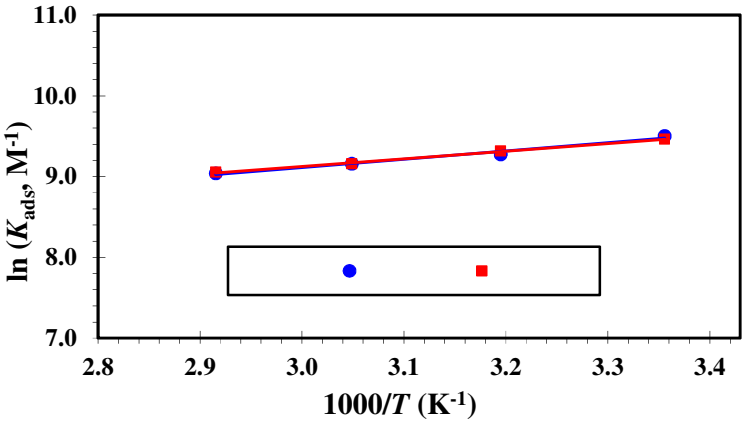

Figure 15: The relation between (ln K_{ads} and 1/T) for carbon steel in different concentrations of the synthesized cationic cationic gemini surfactant.

3.5. Activation energy of the corrosion processes (E_a)

An Arrhenius equation had been employed to calculate E_a values.

$$\ln k = \frac{-E_a}{RT} + \ln A \qquad (12)$$

Where A = Arrhenius constant (pre-exponential factor), R = gas constant (8.314 J mol^{-1}), T = absolute temperature, and K = corrosion rate.

Figs. (16, 17) provide a diagram of ln corrosion rate (k) vs the inverse of temperature (1/T) for CS on 1.0 M HCl With and without varying inhibitor doses. The lines collected have a slope that equals (-E_a/R). Table 5 displays E_a readings, which have been established through analyzing the slope of a linear relationship. In 1M HCl solutions, Inhibitors demonstrate greater activation energy values in comparison to a solution without inhibitors. Increased inhibitor concentrations improved E_a values. This is because the C-steel's surface forms a physical barrier [13, 23]

Table 5: Activation energy (E_a, kJ mol^{-1}) values for carbon steel in 1 M HCl in the absence and presence of different concentrations of both the synthesized Schiff base and cationic gemini surfactant

Conc. of inhibitor (M)	Schiff base	Surfactant
1M HCl	41.68	41.68
1.0×10^{-4}	47.97	46.66
5.0×10^{-4}	49.94	49.51
1.0×10^{-3}	51.40	50.93
5.0×10^{-3}	53.89	53.75

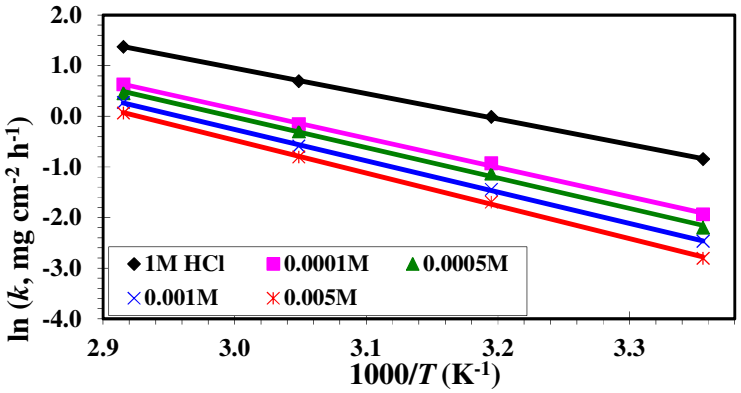

Figure 16: Arrhenius plots for carbon steel dissolution in absence and presence of different concentrations of Schiff.

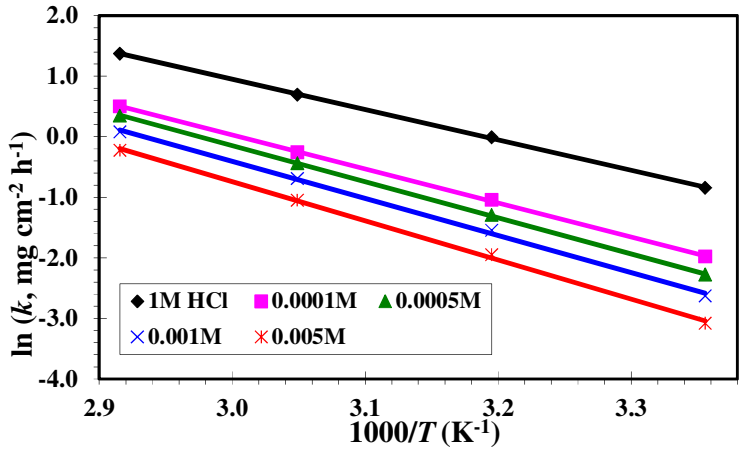

Figure 17: Arrhenius plots for carbon steel dissolution in absence and presence of different concentrations of cationic gemini surfactant.

3.6. Surface-Active Characteristics

3.6.1. Critical Micelle Concentration (C_{cmc}) and Effectiveness (π_{cmc}):

To assess CMC of the generated cationic surfactant, surface tension (γ) was plotted against -log C, as illustrated in Fig. 18. The C_{cmc} values were determined by examining the break point graphs. The following equation was used to calculate effectiveness at C_{cmc} (π_{cmc}), meaning the effect of a surfactant on lowering surface tension.

$$\pi_{cmc} = \gamma_o - \gamma_{cmc} \quad (13)$$

Surface tension of pure water at a certain temperature denoted by γ_o, while γ_{cmc} indicates the surface tension around CMC. Table 6 displays the values for C_{cmc} and π_{cmc}. In the air-water interface, a surfactant is a powerful surface-active agent.

3.6.2. Surface excess (Γcmc)

To compute the maximum surface excess of a surfactant (Γcmc) at the air/solution interface, utilize the slope of the γ versus log C plot before C_{cmc}. In absence of an electrolyte, the calculation is carried out using the Gibbs adsorption equation.

$$\Gamma_{max} = \left(\frac{-1}{nRT}\right)\left(\frac{d\gamma}{d \log C}\right) \quad (14)$$

The expression $d\gamma/d \log C$ shows how quickly the surface pressure is changing in relation to the concentration's logarithm. In this context, R represents the gas constant, T represents the absolute temperature, and the n value is given as 2 for a monomeric surfactant consisting of a divalent surfactant ion and two univalent counter ions. The maximum value of Γ, denoted as Γ_{max}, was computed and documented in Table 6.

3.6.3. Minimum Surface Area (A_{min})

The minimal surface area per adsorbed molecules., A_{min} (nm^2), can be measured using Gibbs adsorption equation:

$$A_{min} = \frac{10^{14}}{N_A \Gamma_{max}} \quad (15)$$

Where Γ_{max} = maximum surface excess of surfactant particles adsorbed on the interface and N_A = The number of Avogadro. The surface area value per molecule was computed and documented in Table 6 [39, 40].

Table 6: Critical micelle concentration (C_{cmc}), effectiveness (π_{cmc}), maximum surface excess (Γ_{max}), and minimum area (A_{min}) values of the synthesized cationic gemini surfactant at 25 °C.

$C_{cmc} \times 10^3$ (mol dm^{-3})	γ_{cmc} (mN m^{-1})	π_{cmc} (mN m^{-1})	$\Gamma_{max} \times 10^{11}$ (mol cm^{-2})	A_{min} (nm^2)
4.78	27	45	9.320	1.78

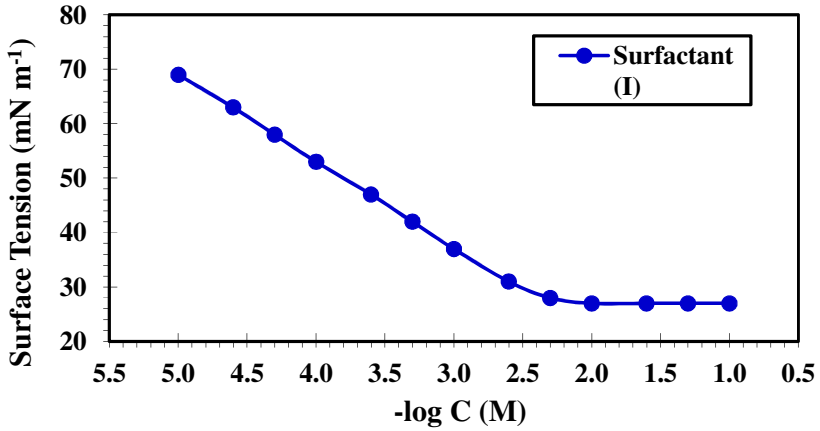

Figure 18: The surface tension variation of different concentrations of the synthesized new cationic gemini surfactant in bi-distilled water at 25 ºC.

3.7. Surface analysis

3.7.1. SEM analysis

The C-steel surface was examined using SEM photomicrographs. which is considered an effective instrument comparable to electrochemical experiments to assess the corrosion performance of C-steel in 1 M HCl with and without inhibitors after a 24-hour immersion time. A micrograph of the surface of C-steel after immersion in a highly acidic solution of HCl (1 M) is displayed in Fig. 19a. The corrosion process caused by the harsh action of HCl caused damage and destruction to the steel [41-43]. Conversely, the addition of $5x10^{-3}$ M of Schiff base, and cationic gemini surfactant (CGS) revealed its anticorrosion behavior as shown in Fig. 19b,c, which depicted C-steel with a noticeably improved surface in comparison to the blank solution. This can be explained by the inhibitor's protection role in C-steel corrosion through the adsorption process and building of an insoluble film layer that reduced the contact between corrosive HCl and C-steel. These findings are in good agreement with the electrochemical results gathered [44, 45].

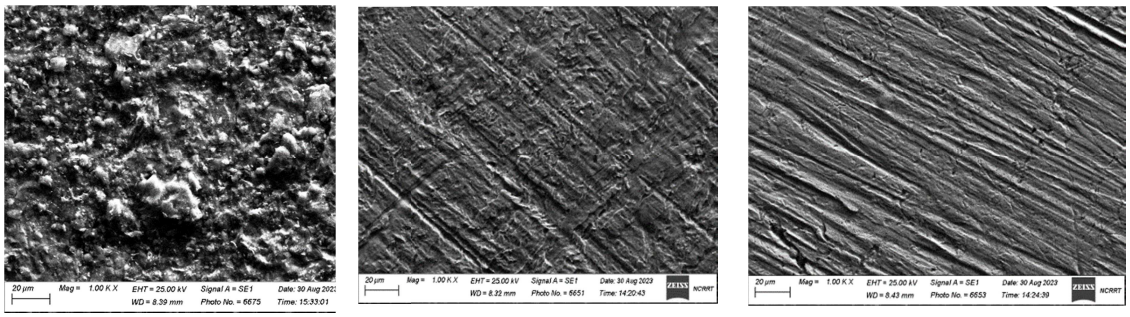

(a) (b) (c)

Figure 19: SEM images of CS in 1M HCl solution at 25 °C: (a) in the absence of the inhibitor, (b) in the presence of Schiff base at 5×10^{-3} M, and (c) in the presence of the CGS at 5×10^{-3} M.

3.7.1. EDX (energy dispersive analysis of X-rays)

Fig. 20a, b, and c display the EDX images of CS samples in 1M HCl with and without inhibitors. The images were captured at a temperature of 25 °C following a 24-hour immersion period. Examining the micrograph, it is evident that the sample submerged in the 1M HCl solution contains chlorine, which is known for its corrosive properties. Meanwhile, the sample immersed in the inhibited solution shows a deficiency of chlorine and displays the carbon and nitrogen atoms of surfactant molecules. This is because the inhibitor species reduce corrosion rate as a result of attaching to metal surfaces and forming protective barrier coatings [30].

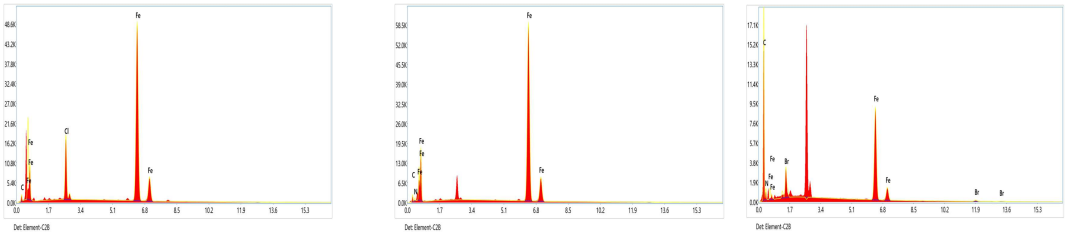

(a) **(b)** **(c)**

Figure 20: EDX chart of CS in 1M HCl solution at 20 °C: (a) in the absence of the inhibitor and (b) in the presence of Schiff base at 5×10-3 M, (c) in the presence of cationic gemini surfactant at 5×10-3 M.

3.8. Mechanism of Corrosion Inhibition.

The inhibitory impact of C-steel in 1 M HCl was confirmed by cationic gemini surfactant, which diminished the surface-to-corrosive acidic solution interaction by forming an insoluble protective film layer. This layer forms as a result of the inhibitor's adsorption process, which covers C-steel with a protective film. The purpose of this layer is to stop corrosion between the electrolyte and the metal. The process of adsorption can be outlined by substituting or replacing H2O molecules on the C-steel surface with inhibitor molecules that accumulate at the metal/solution contact. Cationic gemini surfactants can be adsorbed through electrostatic attraction between charged atoms on their structures and C-steel, as well as chemically through the formation of coordination bonds when electron pairs on heteroatoms or π-electrons of the aromatic/heterocyclic ring react with iron. This interaction reduces the corrosion rate of C-steel, demonstrating that the cationic gemini surfactant works as an efficient inhibitor.

3.9. Comparison of inhibitory efficiencies of some cationic surfactants for carbon steel in acidic solution

Table 7 indicates the inhibitory efficiency of the generated surfactants against carbon steel corrosion in a 1 M HCl solution, as well as several previously reported surfactants. The inhibitory efficiency of the produced cationic surfactants, as indicated in this table, is on par with or even higher than that of cationic surfactants that have previously been reported under identical conditions [14, 46, 47]. Surfactant has low-cost effectiveness than regular organic compounds, and it is easy to create and has low toxicity, making it excellent for the environment [48-56].

Table 7: Some cationic surfactants investigated as corrosion inhibitors by other authors and this work for carbon steel in 1 M HCl (the data obtained by weight loss method) Inhibitor name Inhibition efficiency (%) Reference.

Name of inhibitor (M)	Inhibition efficiency (%)	Reference
(E)-Decyl-4-[(2-hydroxyethylamino) methyl]-N,N dimethyl benzenaminium bromide	**90.26**	**[46]**
(E)-Dodecyl-4-[(2-hydro-xyethylamino)methyl]-N,N dimethyl benzenaminium bromide	**90.95**	**[46]**
(E)-Hexadecyl-4-[(2-hydro-xyethylamino)methyl]-N,N-dimethyl benzenaminium bromide	**93.12**	**[46]**
N,N-bis(2-hydroxyethyl)-N-octylbenzo[d]thiazol 2-ammonium bromide	**87.26**	**[47]**
N,N-bis(2-hydroxyethyl)-N-decylbenzo[d]thiazol 2-ammonium bromide	**91.46**	**[47]**
N,N-bis(2-hydroxyethyl)-N-dodecylbenzo[d] thiazol-2-ammonium	**94.35**	**[47]**

bromide		
N-(3-(benzylideneamino)propyl)-N,N-dimethyldecan-1-ammonium bromide	**82.93**	**[14]**
N-(3-(benzylideneamino)propyl)-N,N-dimethyldodecan-1-ammonium bromide	**87.45**	**[14]**
N-(3-(benzylideneamino)propyl)-N,N-dimethylhexadecan-1-ammonium bromide 88.02	**87.45**	**[14]**
4,4'-((1Z,1'E)-(ethane-1,2-diylbis(azaneylylidene)bis(ethane-1-yl-1-ylidene))bis(1-dodecylpyridin-1-ium) bromide	**94.59**	**Working**

4. Conclusions

1. Mass spectroscopy, ^{1}HNMR, and FTIR were used for chemical analysis of a new cationic gemini surfactant.
2. SCGS was discovered to be a great corrosion inhibitor on 1.0 M HCl. The efficiency of metal corrosion prevention is enhanced as concentration increases and diminishes with rising temperature.
3. Adsorption of inhibitor compounds on CS surfaces creates a layer of protection and results in high inhibitory efficiency of the produced CGS.
4. The inhibitors that were produced have the ability to function as inhibitors of mixed types in 1.0 M HCl.
5. SCGS adsorption on CS surfaces conforms to Langmuir's isotherm. Negatively charged ΔG°_{ads} and ΔH°_{ads} resulted in an exothermic and spontaneous adsorption process. And were accompanied by an entropy rise.
6. SCGS is a suitable surface agent, according to surface tension studies.

5. Conflicts of interest

"There are no conflicts to declare".

6. Formatting of funding sources

List funding sources in a standard way to facilitate compliance to funder's requirements

7. Acknowledgments

Collate acknowledgements in a separate section at the end of the article before the references and do not, therefore, include them on the title page, as a footnote to the title or otherwise. List here those individuals who provided help during the research (e.g., providing language help, writing assistance or proof reading the article, etc.).

8. References and Bibliography

1. Verma, C., et al., A Green and Sustainable Approach for Mild Steel Acidic Corrosion Inhibition Using Leaves Extract: Experimental and DFT Studies. Journal of Bio- and Tribo-Corrosion, 2018. 4(3): p. 33.
2. Obot, I., S. Umoren, and N. Ankah, Pyrazine derivatives as green oil field corrosion inhibitors for steel. Journal of Molecular Liquids, 2019. 277: p. 749-761.
3. Fouda, A.E.-A.S., et al., Corrosion inhibition of carbon steel in hydrochloric acid by cationic arylthiophenes as new eco-friendly inhibitors: Experimental and quantum chemical study. Chinese Journal of Chemical Engineering, 2021. 40: p. 197-217.
4. Feng, L., et al., Cationic Gemini surfactants with a bipyridyl spacer as corrosion inhibitors for carbon steel. ACS omega, 2018. 3(12): p. 18990-18999.
5. Kumar, S., et al., Polyurethane based triblock copolymers as corrosion inhibitors for mild steel in 0.5 M H2SO4. Industrial & Engineering Chemistry Research, 2017. 56(2): p. 441-456.
6. Odewunmi, N., S. Umoren, and Z. Gasem, Watermelon waste products as green corrosion inhibitors for mild steel in HCl solution. Journal of Environmental Chemical Engineering, 2015. 3(1): p. 286-296.
7. Kaczerewska, O., et al., Effectiveness of O-bridged cationic gemini surfactants as corrosion inhibitors for stainless steel in 3 M HCl: Experimental and theoretical studies. Journal of Molecular Liquids, 2018. 249: p. 1113-1124.
8. Hegazy, M., et al., Novel cationic surfactants for corrosion inhibition of carbon steel pipelines in oil and gas wells applications. Journal of Molecular Liquids, 2016. 214: p. 347-356.
9. Finšgar, M. and J. Jackson, Application of corrosion inhibitors for steels in acidic media for the oil and gas industry: A review. Corrosion science, 2014. 86: p. 17-41.
10. Djamel, D., et al., Adsorption and corrosion inhibition of new synthesized thiophene Schiff base on mild steel X52 in HCl and H2SO4 solutions. Corrosion Science, 2014. 79: p. 50–58.

11. Abd El-Maksoud, S.A., et al., New Imidazol-1-ium Bromide Derivative Surfactants as Corrosion Inhibitors for Carbon Steel in 1 M HCl Solutions: Experimental and Theoretical Studies. Journal of Bio- and Tribo-Corrosion, 2021. 7(4): p. 156.
12. Popova, A., et al., AC and DC study of the temperature effect on mild steel corrosion in acid media in the presence of benzimidazole derivatives. Corrosion Science, 2003. 45(1): p. 33-58.
13. Aiad, I., et al., Cationic surfactant based on alignate as green corrosion inhibitors for the mild steel in 1.0 M HCl. Egyptian journal of petroleum, 2018. 27(4): p. 877-885.
14. Aiad, I., et al., Inhibition of mild steel corrosion in acidic medium by some cationic surfactants. Journal of Industrial and Engineering Chemistry, 2014. 20(5): p. 3524-3535.
15. Hegazy, M.A. and A.S. El-Tabei, Synthesis, surface properties, synergism parameter and inhibitive performance of novel cationic gemini surfactant on carbon steel corrosion in 1 M HCl solution. Journal of Surfactants and Detergents, 2013. 16: p. 221-232.
16. Abdallah, M., et al., Adsorption and inhibition performance of the novel cationic Gemini surfactant as a safe corrosion inhibitor for carbon steel in hydrochloric acid. Green Chemistry Letters and Reviews, 2018. 11(4): p. 457-468.
17. Hegazy, M.A., et al., Three novel di-quaternary ammonium salts as corrosion inhibitors for API X65 steel pipeline in acidic solution. Part I: Experimental results. Corrosion Science, 2014. 81: p. 54-64.
18. Migahed, M., M. Hegazy, and A. Al-Sabagh, Synergistic inhibition effect between Cu2+ and cationic gemini surfactant on the corrosion of downhole tubing steel during secondary oil recovery of old wells. Corrosion science, 2012. 61: p. 10-18.
19. Hegazy, M.A., et al., Novel cationic surfactants for corrosion inhibition of carbon steel pipelines in oil and gas wells applications. Journal of Molecular Liquids, 2016. 214: p. 347-356.
20. Mobin, M. and S. Noori, Adsorption and corrosion inhibition behaviour of zwitterionic gemini surfactant for mild steel in 0.5 M HCl. Tenside Surfactants Detergents, 2016. 53(4): p. 357-367.
21. Torres, V., et al., Study of thioureas derivatives synthesized from a green route as corrosion inhibitors for mild steel in HCl solution. Corrosion Science, 2014. 79: p. 108-118.
22. Farag, A.A. and M.N. El-Din, The adsorption and corrosion inhibition of some nonionic surfactants on API X65 steel surface in hydrochloric acid. Corrosion Science, 2012. 64: p. 174-183.
23. Bedair, M., et al., Empirical and theoretical investigations on the corrosion inhibition characteristics of mild steel by three new Schiff base derivatives. Journal of adhesion science and Technology, 2019. 33(11): p. 1139-1168.
24. Faraji, S., et al., The influence of SiC particles on the corrosion resistance of electroless, Cu–P composite coating in 1 M HCl. Materials chemistry and physics, 2011. 129(3): p. 1063-1070.
25. Yıldız, R., et al., Experimental studies of 2-pyridinecarbonitrile as corrosion inhibitor for mild steel in hydrochloric acid solution. Corrosion Science, 2014. 82: p. 125-132.
26. Solmaz, R., Investigation of adsorption and corrosion inhibition of mild steel in hydrochloric acid solution by 5-(4-Dimethylaminobenzylidene) rhodanine. Corrosion Science, 2014. 79: p. 169-176.
27. Qian, B., et al., Synergistic effect of polyaspartic acid and iodide ion on corrosion inhibition of mild steel in H2SO4. Corrosion Science, 2013. 75: p. 184-192.
28. Hegazy, M., et al., Studying the corrosion inhibition of carbon steel in hydrochloric acid solution by 1-dodecyl-methyl-1 H-benzo [d][1, 2, 3] triazole-1-ium bromide. RSC Advances, 2015. 5(61): p. 49070-49079.
29. Asefi, D., M. Arami, and N.M. Mahmoodi, Electrochemical effect of cationic gemini surfactant and halide salts on corrosion inhibition of low carbon steel in acid medium. Corrosion Science, 2010. 52(3): p. 794-800.
30. Hegazy, M. and I. Aiad, 1-Dodecyl-4-(((3-morpholinopropyl) imino) methyl) pyridin-1-ium bromide as a novel corrosion inhibitor for carbon steel during phosphoric acid production. Journal of Industrial and Engineering Chemistry, 2015. 31: p. 91-99.
31. Moradi, M., J. Duan, and X. Du, Investigation of the effect of 4, 5-dichloro-2-n-octyl-4-isothiazolin-3-one inhibition on the corrosion of carbon steel in Bacillus sp. inoculated artificial seawater. Corrosion science, 2013. 69: p. 338-345.
32. Zarrok, H., et al., Corrosion control of carbon steel in phosphoric acid by purpald–Weight loss, electrochemical and XPS studies. Corrosion Science, 2012. 64: p. 243-252.
33. Hegazy, M., et al., Corrosion inhibition performance of a novel cationic surfactant for protection of carbon steel pipeline in acidic media. International Journal of Electrochemical Science, 2018. 13(7): p. 6824-6842.
34. Badr, G., The role of some thiosemicarbazide derivatives as corrosion inhibitors for C-steel in acidic media. Corrosion Science, 2009. 51(11): p. 2529-2536.
35. Dahmani, M., et al., Corrosion inhibition of C38 steel in 1 M HCl: A comparative study of black pepper extract and its isolated piperine. International Journal of Electrochemical Science, 2010. 5(8): p. 1060-1069.
36. El-Tabei, A. and M. Hegazy, Application of the synthesized novel 3, 6, 9, 12, 15, 18, 21-heptaoxatricosane-1, 23-diyl bis (4-((4-(dimethylamino) benzylidene) amino) benzoate) as a corrosion inhibitor for carbon steel in acidic media. Journal of dispersion science and technology, 2014. 35(9): p. 1289-1299.
37. Döner, A., et al., Experimental and theoretical studies of thiazoles as corrosion inhibitors for mild steel in sulphuric acid solution. Corrosion science, 2011. 53(9): p. 2902-2913.
38. Noor El-Din, M., A. Al-Sabagh, and M. Hegazy, Study of the inhibition efficiency for some novel surfactants on the carbon steel (Type H-11) pipelines in 0.5 M HCl solution by potentiodynamic technique. Journal of dispersion science and technology, 2012. 33(10): p. 1444-1451.
39. El-Tabei, A. and M. Hegazy, Synthesis and characterization of a novel nonionic gemini surfactant as corrosion inhibitor for carbon steel in acidic solution. Chemical Engineering Communications, 2015. 202(7): p. 851-863.

40. Labena, A., et al., The biocidal effect of a novel synthesized gemini surfactant on environmental sulfidogenic bacteria: Planktonic cells and biofilms. Materials Science and Engineering: C, 2015. 47: p. 367-375.
41. Zaki, E., M. Abd-El-Raouf, and T. Zidan, Methyl acrylate derivatives as corrosion inhibitors for X-65 type carbon steel in 1 M HCl. International journal of electrochemical science, 2021. 16(3): p. 210374.
42. Elaraby, A., et al., Theoretical and electrochemical evaluation of tetra-cationic surfactant as corrosion inhibitor for carbon steel in 1 M HCl. Scientific Reports, 2023. 13(1): p. 942.
43. El Basiony, N., et al., ρ-Substituted imine cationic surfactants as carbon steel corrosion inhibitors: experimental and theoretical (DFT and MCs) approaches. Journal of Molecular Liquids, 2024. 400: p. 124475.
44. El-Tabei, A., A.E. El-Tabey, and N. El Basiony, Newly imine-azo dicationic amphiphilic for corrosion and sulfate-reducing bacteria inhibition in petroleum processes: Laboratory and theoretical studies. Applied Surface Science, 2022. 573: p. 151531.
45. El Basiony, N., et al., Experimental and theoretical (DFT&MC) studies for the adsorption of the synthesized Gemini cationic surfactant based on hydrazide moiety as X-65 steel acid corrosion inhibitor. Applied Surface Science, 2021. 539: p. 148246.
46. Shaban, S.M., et al., Corrosion inhibition and biocidal effect of some cationic surfactants based on Schiff base. Journal of Industrial and Engineering Chemistry, 2013. 19(6): p. 2004-2009.
47. Badr, E.A., Inhibition effect of synthesized cationic surfactant on the corrosion of carbon steel in 1 M HCl. Journal of Industrial and Engineering Chemistry, 2014. 20(5): p. 3361-3366.
48. Megahed, M.M., M. Youssif, and A.M. El-Shamy, Selective formula as a corrosion inhibitor to protect the surfaces of antiquities made of leather-composite brass alloy. Egyptian Journal of Chemistry, 2020. 63(12): p. 5269-5287.
49. El-Shamy, A.M., A review on: biocidal activity of some chemical structures and their role in mitigation of microbial corrosion. Egyptian Journal of Chemistry, 2020. 63(12): p. 5251-5267.
50. Reda, Y., et al., Effect of plating materials on the corrosion properties of steel alloy 4130. Egyptian Journal of Chemistry, 2020. 63(2): p. 579-597.
51. Megahed, M.M., M.M. Abdel Bar, and A.M. El-Shamy, Polyamide coating as a potential protective layer against corrosion of iron artifacts. Egyptian Journal of Chemistry, 2021. 64(10): p. 5693-5702.
52. El-Shamy, A.M. and M.M. Abdel Bar, Ionic liquid as water soluble and potential inhibitor for corrosion and microbial corrosion for iron artifacts. Egyptian Journal of Chemistry, 2021. 64(4): p. 1867-1876.
53. Saad, W.M. and A. El-Shamy, Unlocking the potential of cinnamaldehyde: a comprehensive study on its dual role as an effective inhibitor against corrosion and microbial corrosion of mild steel in saline environments. Journal of Bio-and Tribo-Corrosion, 2024. 10(1): p. 14.
54. Ghazy, E., N.A. Ghany, and A.M. El-Shamy, Comparative study of cetyl trimethyl ammonium bromide, formaldehyde, and isobutanol against corrosion and microbial corrosion of mild steel in chloride media. Journal of Bio-and Tribo-Corrosion, 2023. 9(3): p. 64.
55. El-Shamy, A.M. and S.M. Mouneir, Medicinal materials as eco-friendly corrosion inhibitors for industrial applications: A review. Journal of Bio-and Tribo-Corrosion, 2023. 9(1): p. 3.
56. Abdel-Karim, A.M., A.M. El-Shamy, and Y. Reda, Corrosion and stress corrosion resistance of Al Zn alloy 7075 by nano-polymeric coatings. Journal of Bio-and Tribo-Corrosion, 2022. 8(2): p. 57.